Large-scale Climate Variability Footprint in Water Levels of Alluvial Aquifers Across Iran

Abolfazl Rezaei (abolfazlrezaei64@gmail.com)
Institute for Advanced Studies in Basic Sciences https://orcid.org/0000-0001-8619-2442

Research Article

Keywords: Iran's principal aquifers, Atlantic and Pacific atmospheric oscillations, Climate and groundwater variability, Wavelet analysis

Posted Date: September 13th, 2021

DOI: https://doi.org/10.21203/rs.3.rs-331415/v1

Version of Record: A version of this preprint was published at Theoretical and Applied Climatology on January 8th, 2022. See the published version at https://doi.org/10.1007/s00704-021-03920-6.

Large-scale climate variability footprint in water levels of alluvial aquifers across Iran

Abolfazl Rezaei[1, 2]

[1] Department of Earth Sciences, Institute for Advanced Studies in Basic Sciences (IASBS), Zanjan 45137–66731, Iran; arezaei@iasbs.ac.ir; abolfazlrezaei64@gmail.com.

[2] Center for Research in Climate Change and Global Warming (CRCC), Institute for Advanced Studies in Basic Sciences (IASBS), Zanjan, Iran

Abstract

The ability to predict future variability of groundwater resources in time and space is of critical importance in society's adaptation to climate variability and change. Periodic control of large scale ocean-atmospheric circulations on groundwater levels proposes a potentially effective source of longer term forecasting capability. In this study, as a first national-scale assessment, we use the continues wavelet transform, global power spectrum, and wavelet coherence analyses to quantify the controls of the Atlantic Multidecadal Oscillation (AMO), Pacific Decadal Oscillation (PDO), North Atlantic Oscillation (NAO), and El Niño Southern Oscillation (ENSO) over the representative groundwater levels of the 24 principal aquifers, scattered across different 14 climate zones of Iran. The results demonstrate that aquifer storage variations are partially controlled by annual to interdecadal climate variability and are not solely a function of pumping variations. Moreover, teleconnections are observed to be both frequency and time specific. The significant coherence patterns between the climate indices and groundwater levels are observed at five frequency bands of the annual (~1-yr), interannual (2-4- and 4-6-yr), decadal (8-12-yr), and interdecadal (14-18yr), consistent with the dominant modes of climate indices. AMO's strong footprint is observed at interdecadal and annual modes of groundwater levels while PDO's highest imprint is seen in

interannual, decadal, and interdecadal modes. The highest controlling influence of ENSO is observed across the decadal and interannual modes whereas the NAO's footprint is marked at annual and interdecadal frequency bands. Further, it is observed that the groundwater variability being higher modulated by a combination of large-scale atmospheric circulations rather than each individual index. The decadal and interdecadal oscillation modes constitute the dominant modes in Iranian aquifers. Findings also mark the unsaturated zone contribution in damping and lagging of the climate variability modes, particularly for the higher frequency indices of ENSO and NAO where the groundwater variability is observed to be more correlated with lower frequent climate circulations such as PDO and AMO, rather than ENSO and NAO. Finally, it is found that the data length can significantly affect the teleconnections if the time series are not contemporaneous and only one value of coherence/correlation is computed for each particular series instead of separate computations for different frequency bands and different time spans.

Keywords: Iran's principal aquifers; Atlantic and Pacific atmospheric oscillations; Climate and groundwater variability; Wavelet analysis

1. Introduction

The potential impacts of natural climate variability upon water resources on local to global scales have been an increasingly crucial water management subject (Velasco et al., 2015) since climate variability plays an essential role in the sustainability of water resources (Sadoff and Muller, 2009). Periodic control of ocean-atmospheric circulations over groundwater levels offers a potentially important source of longer term forecasting capability that is of critical importance to drought management (Rust et al., 2018). Despite the effect of interannual to multidecadal climate variability on the spatiotemporal distribution of precipitation, drought, groundwater and surface-water storage variations (Ropelewski and Halpert, 1986; Cayan and Webb, 1992; Hurkmans et al., 2009; Sadoff and Muller, 2009; Vicente-Serrano et al., 2011, Kuss and Gurdak, 2014; Rezaei and

Gurdak, 2020, Rezaei, 2020), it is still poorly understood how climate variability modulates subsurface hydrologic processes and groundwater storage worldwide (Hanson et al., 2006; Green et al., 2011; Kuss and Gurdak, 2014; Velasco et al., 2015; Rust et al., 2018). As the largest accessible freshwater resource, groundwater has a critical role in providing adequate water supplies for human consumption, agricultural and industrial purposes, and ecosystem function (Treidel et al., 2012). Subsurface hydrologic response to natural climate variability is of particular interest in semiarid and arid climates, where groundwater resource availability and sustainability are crucial (Hanson et al., 2004). Groundwater supplies the primary source of freshwater in a broad portion of Iran where the groundwater pumping from production wells provided solely ~60% of the entire water supply across the nation (Mirzaei et al., 2019). Therefore, understanding how climate variability influences groundwater resources in Iran with (semi)arid climate is essential for sustainable development and management of groundwater and surface-water resources (Hanson et al., 2004; Kuss and Gurdak, 2014; Velasco et al., 2015; Rezaei and Gurdak, 2020).

Despite the importance of groundwater resources, few investigations have documented the teleconnections between large-scale climate indices and natural variability in Iranian aquifers. Rezaei and Gurdak's (2020) study was the first in Iran to quantify the effects of large-scale climatic variability on groundwater resources, by examining the influence of ENSO, NAO, PDO and AMO on interannual (>2-year) to interdecadal modes of groundwater levels from aquifers surrounding the Lake Urmia. In that study, we found that the Pacific-based climate oscillations (PDO and, to lesser magnitude, ENSO) have a more powerful influence than the Atlantic-based oscillations (NAO and AMO) on the variability in the groundwater levels. Moreover, Rezaei (2020) explored the teleconnection between ENSO and PDO climate indices and a karst Sarabkalan Spring's discharge in the southwest of Iran with a fast-slow flow system. In this work, evidence is presented which shows a positive PDO phase coupled with El Nino increased both the precipitation and spring discharge.

In this paper, we quantify the teleconnections between AMO, PDO, NAO, and ENSO and the groundwater levels of 24 principal aquifers scattered over the country. Iran, as a country with a highly variable climate, is categorized into 14 different climate zones (Alizadeh-Choobari and Najafi, 2018). The primary objective of this paper is to characterize nonstationary patterns in climate variability to spatiotemporal trends in groundwater level records (16–52 years) from 24 principal aquifers across Iran. This paper is the first national-scale study to capture signatures of the interannual to multidecadal climate variability controls on groundwater storage in Iran and enhances current understanding required for better water resources management and policy decisions under increasing climate uncertainty. Moreover, the influence of data length on the teleconnections between climate indices and groundwater levels are assessed.

2. Study area

Iran with ~82 million inhabitants and 1,648,195 km^2 in the area is the second-largest country in the Middle East. Different regions have different climate conditions so that Iran has been classified into 14 climate zones by Alizadeh-Choobari and Najafi (2018) based on the principal component analysis with varimax rotation applied on the 21 meteorological variables such as mean annual precipitation, temperature, and humidity. The country's climate varies from mild and humid in the southern coasts of the Caspian Sea with mean annual precipitation of >1000 mm to warm and arid in the central-to-east parts with mean annual precipitation of <125 mm. The selected aquifers mapped on the 14 climate zones across the country are shown in Fig. 1. The full description of these 14 climate zones is presented by Alizadeh-Choobari and Najafi (2018). The minimum annual temperature over Iran varies from -2.8°C across northwestern Iran, Zagros Mountains, and some parts of Kerman Province (containing aquifer 9c), to +33.8°C at the northern coasts of the Persian Gulf and the Oman Sea (Hadi Pour et al., 2019). The highest annual precipitation falls over the southern coasts of the Caspian Sea (up to ~1850mm) whereas its lowest values (<125mm) occur in arid regions of central, southern, southeastern (Fig. S1 in Supporting Information (SI)). This highly variable climate is

triggered by the climate impacts imposed by the geographical position of sea/gulf and land in the continent and the mountain ranges (Alborz and Zagros) that border two extremely arid deserts in central Iran (i.e., Kavir and Lut). The Zagros and Alborz act as a low-level air mass barrier for the flow of moisture that comes from west-to-southwestern Iran and the Caspian Sea towards central Iran (Alijani, 2000). In this study, we selected 24 different principal aquifers (Fig. 1 and Table 1), at least one from each climate zone, to scrutinize their links with large scale ocean-atmospheric circulations. These aquifers are selected based on the length and continuity of representative water-level records. The selected aquifers are at different mean elevations from ~2 (aquifer 3 at the southern coast of the Caspian Sea) to 2268 m.a.b.s.l (aquifer 6b in the Zagros Mountains). The aquifers have a highly variable range of mean water table depth from less than 10 m (aquifers 3 (2.8 m), 2 (3 m), 4 (6.3 m), 5 (8.3 m), and 13 (7.2 m)) to more than 50 m (aquifers 9c (68 m), 7c (58.5 m), and 9b (52.7 m)). Overall, the shallowest aquifers are located at the coasts of the Caspian Sea (with the highest precipitation) and the Lake Urmia while the deepest ones are almost placed in central Iran (with the lowest rainfall).

Table 1. The summary of the general characteristics of the 24 aquifers selected for this study.

Aquifer	ID	Area (km^2)	Mean elevation (m)	Mean water table depth (m)	Data length (year)	Climate zone	Aquifer group
Ardabil	1a	970	1467	19.0	46.9	1	G1
Tabriz	1b	1200	1582	19.6	34.9		
Kabodar-Ahang	1c	1470	1819	33.0	29.9		
Mahaba	2	175	1320	3.0	21.9	2	G2
Laijan-Chaboksar	3	850	2	2.8	30.9	3	G3
Babol-Amol	4	1405	72	6.3	27.9	4	G4
Gorgan	5	4395	409	8.3	45.9	5	G5
Ghorveh-Dehgolan	6a	1270	1932	20.0	31.9	6	G6
Brojen	6b	215	2268	15.5	33.9		
Dorod-Brojerd	6c	487	1893	10.2	20.9		
Shirvan	7a	750	1250	45.8	24.9	7	G7
Ghazvin	7b	3955	1435	40.0	51.8		
Mashhad	7c	2527	1521	58.5	33.9		
Dashte-Abbas	8a	200	189	22.8	32.9	8	G8

Shiraz	8b	452	1790	23.6	24.9		
Kashan	9a	1737	1143	32.0	27.9	9	G9
Esfahan-Barkhorda	9b	1643	1650	52.7	35.9		
Kerman-Baghin	9c	2025	1955	68.0	31.9		
Dastgordan	10a	1027	945	31.4	24.9	10	G10
Damghan	10b	1577	1433	44.6	23.9		
Mosafer-Abad	11	739	445	45.5	25.9	11	G11
Mirjaveh	12	611	1132	45.0	32.9	12	G12
Ramhormoz	13	756	174	7.3	16.9	13	G13
Pirsohrab-Ouraki	14	261	72	32.5	16.0	14	G14

3. Methodology:

Here, we use the monthly time series from AMO, PDO, NAO, and Southern Oscillation Index (SOI) indices (Fig. S2) along with monthly representative groundwater levels from 24 aquifers listed in Table 1. Note that SOI is the oldest indicator for ENSO in which the positive and negative values are associated with La Nina and El Niño, respectively. The monthly times series of the climate indices of AMO, PDO, NAO, and SOI were downloaded from National Oceanic and Atmospheric Administration (NOAA). We selected the principal unconfined aquifers with the longest continuous data length from each climate zone. The representative water table times series for each aquifer was taken from Iran Water Resources Management Company, Tehran. It is necessary to acknowledge that some of the variability in the groundwater level records could be related to human activities and not solely a function of natural climate patterns owing to dry season pumping from aquifers (Hanson et al., 2004; Rezaei and Gurdak, 2020).

The simple flowchart of the methodology is shown in Fig. 2. We first removed the long-term trend of each groundwater level series by subtracting a regression-fitted low-order polynomial using a computer program of the USGS Hydrologic and Climate Analysis Toolkit, HydroCLimATe (Dickinson et al., 2014). Notably, the detrending can (1) partially eliminate the anthropogenic signals (such as groundwater extraction and other water resources development), (2) the red noise from the original

records before using SSA to capture the temporal structure of the data series successfully (Kuss and Gurdak, 2014), and (3) much of the long-term, multidecadal anthropogenic signals (e.g., groundwater extraction and crop irrigation) from the groundwater level series (Gurdak et al., 2007; Hanson et al., 2004).

The wavelet analysis conducted here has four methodological steps of the local continuous wavelet transform (CWT), the cross-wavelet transform (XWT), the wavelet coherence (WTC), and multiple wavelet coherence (MWTC). The local CWT ($W_n^X(s)$ for a time series (x_n, n=1,. . . ,N) with uniform time steps δt, has been defined as the convolution of x_n with the scaled and normalized wavelet (Grinsted et al. 2004):

$$W_n^X(s) = \sqrt{\frac{\delta t}{s}} \sum_{n'=1}^{N} x_{n'} \psi_0 \left[(n'-n) \frac{\delta t}{s} \right], \psi_0(\eta) = \pi^{-1/4} e^{i\omega_0 \eta} e^{-0.5\eta^2} \quad (1)$$

where ψ_0 is the Morlet wavelet, (*) the complex conjugate, s the wavelet scale, ω_0 dimensionless frequency, and η dimensionless time. To test the significance of CWT, 1000 randomly constructed synthetic series were generated by Monte Carlo methods (Grinsted et al., 2004). Furthermore, the global power spectrum, GPS (as a function of time) for each time series was also computed using a MATLAB script written by Schulte (2019). The degree to which the power spectrum exceeds the background noise was assessed by cumulative arcwise significant test (95% confidence bound). The cross wavelet transform (XWT) for each pair of time series (i.e., x_n and y_n) was defined as $W^{XY} = W^X W^{Y*}$, where * is complex conjugation. Finally, WTC for each pair of time series is calculated as follows (Torrence and Webster, 1999; Grinsted et al., 2004):

$$R_n^2(s) = \frac{\left| S\left(s^{-1} W_n^{XY}(s)\right) \right|^2}{S\left(s^{-1} \left|W_n^X(s)\right|^2\right) . S\left(s^{-1} \left|W_n^Y(s)\right|^2\right)}, S(W) = S_{scale}(S_{time}(W_n(s))) \quad (2)$$

where $S(W)$ is a smoothing operator, S_{scale} smoothing along the wavelet scale axis, and S_{time} smoothing in time. The CWT was applied to define the dominant oscillation modes of each individual series (Grinsted et al., 2004). Next, the XWT was used for each time series to depict the cross-wavelet power of a pair series against the background power spectra (Torrence and Compo, 1998; Grinsted et al., 2004). A cone of influence (COI) is used to characterize the zone of the wavelet spectrum in which these edge impacts need to be excluded (Torrence and Compo, 1998; Grinsted et al., 2004). The cross-correlation (ranges from 0 to 1) between a pair series as a function of frequency was computed by the WTC. Finally, to test the significance of the WTC, 1000 randomly constructed synthetic series were generated by Monte Carlo methods (Grinsted et al. 2004).

The multiple wavelet coherence (MWTC) at scale s and location τ can be formulated as (Hu and Si, 2016):

$$\rho_m^2(s,\tau) = \frac{\overset{\iota}{W}^{Y,X}(s,\tau)\overset{\iota}{W}^{X,X}(s,\tau)^{-1}\overline{\overset{\iota}{W}^{Y,X}(s,t)}}{\overset{\iota}{W}^{Y,Y}(s,\tau)} \quad (3)$$

where $\overset{\iota}{W}^{Y,X}(s,\tau)$ is the smoothed cross-wavelet power spectrum between multiple predictor variables *X* and response variables *Y*, $\overset{\iota}{W}^{X,X}(s,\tau)$ signifies either the smoothed auto-wavelet power spectra for the main diagonal of the matrix (i.e., $i = j$) or cross-wavelet power spectra when $i \neq j$, and $\overline{\overset{\iota}{W}^{Y,X}(s,\tau)}$ is complex conjugation $\overset{\iota}{W}^{Y,X}(s,\tau)$. The MWTC at the 95% confidence level was also computed by the Monte Carlo method (Grinsted et al., 2004).

4. Results:

4.1. Continuous wavelet transform (CWT):

Fig. 3 shows the CWT and GPS results for both the climate indices (AMO, PDO, NAO, and ENSO) and the groundwater level series. AMO has significant power regions at three frequency bands of annual (particularly after 1998 in the local CWT), decadal (8-10-yr, particularly after 1980 in both

the local and GPS), and interdecadal (>16-yr as peak signal in GPS). In both the CWT and GPS, PDO also has significant power regions across the three frequency bounds of interannual (4-6-yr), decadal (8-12-yr), and, to lesser magnitude, interdecadal (>16-yr). Significant power regions for NAO are observed at annual, interannual (6-10-yr), and, to smaller magnitude, interdecadal (>16-yr) modes. For ENSO, there are two significant power patterns at interannual (2-7-yr) and decadal (10-13-yr) frequency bands. Notably, the power patterns from the Pacific-based indices (PDO and ENSO) are stronger than those from the Atlantic-based ones (AMO and NAO).

When used to the representative groundwater levels from the 24 aquifers, the local CWT and GPS analyses (Fig. 3) identified significant natural variability at annual (1-yr), interannual (2-7-yr), and decadal-interdecadal (8-18-yr) frequency bands, consistent with climate indices. Except for aquifers 11-14 which we couldn't compute the interdecadal periodicities owing to the lack of data length, it seems that annual and interdecadal oscillation signals are the most dominant modes in the majority of the aquifers. Likewise, the dominant power regions in the integrated precipitation and soil-moisture time series over Iran have occurred from the interannual to interdecadal (Rezaei, 2021). For the groundwater in the Lake Urmia catchment, Rezaei and Gurdak (2020) reported that the interannual oscillations are more related to ENSO and lesser to NAO while the decadal-interdecadal modes are largely originating from PDO. They removed the signals with periodicities of less than 2 that resulted in significant loss of the annual signals, while the local CWTs here demonstrate that the annual signals in most cases are distributed over the whole transect, signifying the importance of annual modes. The commonality in results of CWT analyses from groundwater here and both precipitation and surface soil-moisture by Rezaei (2021) suggests that these hydroclimate variables are responding to a common coherent signal, being driven by the same mechanism or drivers (i.e., large scale oceanic-atmospheric teleconnections). This is further supported by a similarity between the interannual signals from hydroclimate variables and dominant

198 frequencies from ENSO, PDO, and NAO and similarity between the interdecadal signals from
199 hydroclimate variables and dominant modes in PDO and AMO.

200 **4.2. Wavelet Coherence (WTC):**

201 We examined the links between groundwater level and climate indices of AMO, PDO, NAO,
202 and ENSO by computing WTC to visually illustrate both those frequency bands and time intervals at
203 which climate indices and groundwater levels series are covarying (Torrence and Webster, 1999).
204 Significant coherence is depicted in each run of the WTC analysis, where contours enclose statistically
205 significant periods ($P<0.05$), based on a red-noise process as determined by a Monte Carlo
206 experiment (Grinsted et al., 2004). Fig. S3 shows the 96 WTC's runs computed for teleconnections
207 between 24 aquifers and four climate indices of AMO, PDO, NAO, and ENSO. For brevity, the results
208 for all 14 aquifer groups are elaborated in section "WTC analyses in more details" in SI and here we
209 only present the general findings. Consistent with the dominant modes obtained from the CWT
210 modes (Fig. 3), observations demonstrate that the significant coherence patterns between the
211 climate indices and groundwater levels, on the whole, are occurred at five frequency bands of the
212 annual (~1-yr), short-interannual (2-4-yr), middle-interannual (4-6-yr), decadal (8-12-yr), and
213 interdecadal (14-18-yr). Hereafter, for brevity, we use these terms for dominant modes without
214 referring to the corresponding year bands. To statistically assess and easily compare the results, the
215 coherence values from all the 24 aquifers are averaged across each of the significant frequency bands
216 (Fig. 4).

217 The annual variability in the groundwater levels from all the 24 aquifers is highly correlated
218 to AMO (mean coherence value of 0.58) and, to lesser magnitude, PDO (0.47) and NAO (0.45). ENSO
219 (0.32) shows the lowest coherence with annual frequency signals (Fig. 4a). The mean coherence
220 value between AMO and water level across annual mode is computed to be ≥0.70 for aquifers 8b
221 (0.80), 2 (0.80), 6c (0.79), 7a (0.77), 1c (0.76), 6a (0.73), 13 (0.72), 7c (0.72), 6b (0.71), 1b (0.70),

suggesting the critical importance of the annual variability. The AMO's coherence with annual signals of the water levels is highly stronger from 1998 to 2019 compared to the latest 30-year of the 19th century. As a case example, Fig. 5 shows the strong coherence patterns across annual bands of the WTCs for aquifers 1c, 6c, and 8b.

For interannual frequency bands, the significant coherence patterns have occurred at 4-6-yr (in most cases) and 2-4-yr (in some cases) periods (Fig. S3). For all aquifers, the mean coherence value at the 2-4-yr frequency bands for ENSO (i.e., SOI), AMO, PDO, and NAO is equal to 0.38, 0.35, 0.33, and 0.33, respectively (Fig. 4). The significant coherence patterns across the 2-4-yr modes are more apparent in the groundwater levels of Caspian Sea's southern coast (i.e., aquifers 3 and 4), western Zagros (aquifers 6a, 6b, and 6c), and northern coasts of the Persian Gulf (aquifers 13 and 8b) and the Oman Sea (aquifer 14) (Fig. S3). Although in Fig. 4a, the mean values of coherence over all the aquifers from PDO (the mean coherence value of 0.44), ENSO (0.43), NAO (0.43), and AMO (0.40). Both the PDO and ENSO are close to each other, based on the extend and significant level of the observed patterns in the WTCs (Fig. S3), the interannual 4-6-yr signals of groundwater levels, in decreasing order, are controlled by PDO, ENSO, NAO, and AMO. Both the PDO and ENSO usually have the same coherence patterns at the interannual 4-6-yr periods in the WTCs (Fig. S3), particularly in groundwater levels from northwestern Iran (aquifers 1b, 1c, 3, and 7b), western Zagros (aquifers 6a, 6b, 6c, and 8a), and northeastern Iran (aquifers 7a and 7c). Consistent with the significant interannual power regions in the CWT for ENSO (Fig. 3), the coherence patterns of ENSO and PDO at the WTCs have a larger extend across the periods of before 2000 and after 2010; the former is more apparent in most aquifers such as 1a, 1b, 2, 4, 6b, 7a, 7c, 8a, 9c, and 12 and the latter is more stronger in the aquifers of 1b, 1c, 2, 3, 6c, 7b, 7c, 8b, 9c, 11, 12, and 14 (Fig. S3). At the interannual 4-6-yr signals, NAO has the highest coherence with aquifers of 6b, 7a, 7b, 8a, and 9c (Fig. S3). Notably, aquifers 7a and 7b are located in northeastern Iran (upper latitudes) where its precipitation and soil-moisture are previously reported to be more correlated with NAO (Rezaei, 2021). AMO relatively has

247 higher coherence with water levels of the northern (aquifers 1b, 1c, 6c, 7a, and 7c) and the central
248 (aquifers 9a and 9c) parts of the country.

249 Consistent with the significant power regions across the decadal signals shown in the CWTs
250 (Fig. 3), Fig. 4a further demonstrates that the decadal signals from the groundwater levels are more
251 correlated with the Pacific-based indices of ENSO (mean coherence value of 0.64) and PDO (0.63)
252 rather than the Atlantic-based indices of NAO (0.41) and AMO (0.37).

253 The above observations show that each dominant mode in groundwater levels is significantly
254 affected by more than a single climate index. Furthermore, Wyatt et al (2012) found significant co-
255 variances between all North Atlantic indices, and Rezaei (2021) revealed that the interacting effects
256 of ENSO+PDO+NAO on integrated precipitation and soil-moisture across Iran are larger than each of
257 the individual indices. Therefore, we further examined the multiple interacting effects from some
258 combinations (two- and three-coupled) of the most effective indices by computing the MWTC. Figs.
259 4b and 4c examine the multiple interacting effects from some combinations (two- and three-coupled)
260 of the most effective indices by computing the MWTCs. Here we select the two-coupled indices in a
261 manner to compare the integrated effects of the pacific-based (PDO and ENSO) with Atlantic-based
262 (AMO and NAO) indices as well as compare the indices of the dominant interannual periodicities
263 (ENSO and NAO) with those of dominant interdecadal modes (AMO and PDO). For the three-coupled
264 indices, Fig. 4c only shows the most three important multiple indices of AMO+NAO+PDO,
265 AMO+PDO+SOI, and NAO+PDO+SOI that observed to have the highest and broadest coherence
266 patterns with groundwater levels. Figs. 4b and 4c demonstrate that the multiple indices over the
267 annual, decadal, and interannual dominant periodicities have the highest coherence with
268 groundwater levels in Iranian aquifers compared to single indices (Fig. 4a).

269 Figs. 5 and S3 show that the interdecadal signals are more correlated with the lower-
270 frequency indices of AMO (mean coherence value of 0.71) and PDO (0.62) rather than the higher-

frequency indices of ENSO (0.29) and NAO (0.29). Given the limit of data length, the interdecadal patterns are only captured in the three aquifers of 1a, 5, and 7b to the northern parts of the country. The significant coherence patterns between AMO and PDO indices and groundwater levels in both aquifers 1a and 7b (in northwestern Iran) are stronger than aquifer 5 (southeastern coasts of the Caspian Sea). Although AMO and PDO have stronger footprint in the interdecadal signals of the water levels, ENSO can be considered as a weaker counterpart since there are moderate to strong coherence patterns between ENSO and water levels, particularly before 2000.

5. Discussion:

5.1. Teleconnections between climate indices and groundwater level

Understanding the nature of annual to interdecadal variability in groundwater storage and their coupling and responding to climate patterns provides insight into how aquifers may respond to climate variability and their potential susceptibility to change. To see in which part of the country, groundwater is more affected by climate indices, in addition to the WTC analysis, we computed the mean coherence values over the five significant frequency bands (annual to interdecadal) from all the WTCs between climate indices and aquifers (Fig. 6). This study indicates the groundwater levels in Iran partially control by natural climate variability and are not solely a function of temporal patterns in pumping since the wavelet transforms indicate significant coherence between AMO, PDO, NAO, and ENSO indices and water levels in many of aquifers. This partial control of natural climate variability on groundwater storage has also been reported from different parts of the world such as the USA, Canada, and Europe (e.g., Hanson et al., 2004; Perez-Valdivia et al., 2012; Kuss and Gurdak, 2014; Velasco et al., 2015; Rust et al., 2019). Overall, the ocean-atmospheric circulations have relatively highest effects on the western Zagros (mean coherence value of 0.54 for group G6), northeastern (0.48 for group G1), northern (0.47 for group G3 and 0.45 for group G4), and northeastern (0.46 for group G7) regions of the country, respectively. The highest linkages are

related to the Zagros and upper latitude regions of the country where relatively have the shallowest water table, highest precipitation, and lowest temperature. On the contrary, the lowest teleconnections are observed in the aquifers of the southeastern (0.29 in group G12), and the central to eastern (from central Iran, G10 (0.34), to the northern coasts of the Persian Gulf G11 (0.40)) portions. Furthermore, Alizadeh-Choobari and Najafi (2018) reported that ENSO has the lowest correlation with precipitation in southeastern Iran. Possible reasons for this are (1) northern Iran and western Zagros are of the highest annual precipitation across the country while the eastern and southeastern portions receive the lowest annual precipitation (<150mm/yr), and (2) the shallowest aquifers are almost located in the northern Iran and western Zagros while the aquifers across the eastern and southeastern Iran tend to have thicker unsaturated zones with a larger damping and lagging contributions. In fact, the arid climate may create strong upward total potential gradients in the unsaturated zone that decrease downward water flux resulted from current climate variability (Walvoord et al., 2003; McMahon et al., 2007). Consequently, the linkage between atmospheric circulations and Iranian aquifers generally weakens from the upper latitudes (particularly, the northwest and western Zagros regions) to lower latitudes (especially, southwestern Iran) with drier conditions.

The other notable observation that can be made is the teleconnection between the climate indices and each groundwater level is frequency specific. In other words, an individual index may have higher influence at a specific frequency band while it doesn't show any strong footprint in other frequency bands. In Iranian aquifers, the WTCs results from different frequency bands indicate that there are five bands with significant coherence patterns including annual, short-interannual, middle -interdecadal, decadal, and interdecadal, consistent with the significant power regions in the CWTs (Fig. 3). In each significant frequency-band, only one or two climate indices are largely effective. The annual signals largely correlate with AMO and, to lesser magnitude, PDO and NAO. The significant imprints of AMO in Iran's precipitation and drought have also been postulated (Ahmadi et al., 2018;

Mohammadrezaei et al., 2020). Ahmadi et al. (2018) reported that both the ENSO and AMO largely correlate with Iran's precipitation. It has also been observed that AMO has a significant effect on temperature across northwestern Iran (Abbasi and Malek, 2017; Rezaei and Gurdak, 2020). Nonetheless, we observed that ENSO has the lowest correlation with annual signals of groundwater levels while the significant control of ENSO on hydroclimate variables (not groundwater levels) has been previously reported in the literature (e.g., Alizadeh-Choobari and Najafi, 2018; Ahmadi et al., 2019; Alizadeh-Choobari and Adibi, 2019). The possible reason for this is the damping and lagging effects of the unsaturated zone elaborated in the last part of this section.

For the interannual frequency bounds, the significant coherence patterns between climate indices and aquifer's water level have occurred at modes of short-interannual (in most cases) and middle-interannual (in some cases) (Fig. S3). At the short-interannual mode, although the WTC's for AMO, PDO, and NAO indices show relative coherence with groundwater levels, ENSO has a higher coherence with aquifers because of that the significant power spectrums at short-interannual mode for ENSO is highly stronger than those for other indices (Fig. 3). At the short-interannual signals, both the PDO and ENSO have relatively stronger influences on groundwater levels compared to NAO and AMO since beyond the larger mean coherence values (Fig. 4), they show the larger extent and stronger significant coherence patterns at the WTCs (Fig. S3). We attribute the stronger coherence patterns of the middle-interannual oscillations to either the higher damping of climate signals through the unsaturated zone (Velasco et al., 2015; Rust et al., 2018) or the presence of stronger middle-interannual modes in both the PDO and ENSO compared to the short-interannual signals (Fig. 3). In the short-interannual signals, both the PDO and ENSO usually have the same coherence patterns with water levels, particularly in northwestern Iran (aquifers 1b, 1c, 3, and 7b), western Zagros (aquifers 6a, 6b, 6c, and 8a), and northeastern Iran (aquifers 7a and 7c) (Fig. S3). Consistent with the significant interannual power spectrums in the CWT analyses for SOI (Fig. 3), the coherence patterns between SOI and groundwater are stronger before 2000 in most aquifers include 1a, 1b, 2,

4, 6b, 7a, 7c, 8a, 9c, and 12 and after 2010 in the aquifers of 1b, 1c, 2, 3, 6c, 7b, 7c, 8b, 9c, 11, 12, and 14. This similarity between ENSO and PDO's coherence patterns relies on the synergy between ENSO and PDO that is discussed by Newman et al. (2003) and Juanxiong et al. (2004). It appears to be in good agreement with the combined strong footprints of ENSO and PDO on Iran's drought (Rezaei, 2021) and on soil-moisture and dust across the Fertile Crescent, an area contains Iraq, Syria, Jordan, Israel, and western Iran (Notaro et al., 2015). Furthermore, the significant correlation between ENSO and hydroclimate variables across Iran has been previously postulated (Alizadeh-Choobari and Najafi, 2018; Ahmadi et al., 2019; Alizadeh-Choobari and Adibi, 2019; Rezaei and Gurdak, 2020).

Consistent with the significant power spectrums at the decadal oscillations in the CWTs (Fig. 3), Fig. 4 further demonstrates that the decadal signals from the groundwater levels are more correlated with the Pacific-based indices of ENSO (0.64) and PDO (0.63) rather than NAO (0.41) and AMO (0.37). Likewise, Rezaei (2021) demonstrated that the highest coherence between ENSO and PDO indices and Iran's integrated precipitation and soil-moisture has occurred in two bands of 4-7-year and ~>10-year. Similar to the 4-6-yr signals, both the ENSO and PDO also show similar significant coherence patterns at the decadal oscillation signals for almost aquifers such as 1a, 1b, 1c, 3, 4, 5, 6a, 6b, 7b, 7c, 8b, 9a, 9c, 10b, 11, and 13 (Fig. S3). These aquifers are roughly distributed at a broad portion of the country, signifying that the decadal oscillations are one of the dominant signals in groundwater systems that are highly controlled by natural ocean-atmospheric circulations, particularly those from the Pacific Ocean. The CWT results (Fig. 3) also show that the decadal oscillations are the dominant signals observed in both the climate indices of ENSO and PDO as well as in most of the above aquifers. It is noted that because the decadal oscillation is likely the most dominant mode in the original ENSO and PDO time series that are also highly larger than those in AMO and NAO, ENSO and PDO have stronger control on the decadal signals of the water levels than the Atlantic-based indices of AMO and NAO.

Both the mean coherence values (Fig. 4a) and the significant coherence patterns at the WTCs (Fig. S3) indicate that beyond the decadal modes, the interdecadal oscillations are also dominant modes in Iranian aquifers. The interdecadal signals in the water level measurements are reasonably more correlated with the lower-frequency indices of AMO (0.71) and PDO (0.62) compared to the higher-frequency indices of ENSO (0.29) and NAO (0.29) (Figs. 5 and S3), because of low-frequency signals tend to be preserved better in groundwater fluctuations than high-frequency signals (Velasco et al., 2015). Likewise, the higher influence of the lower-frequency index of PDO on groundwater systems is found for the U.S. West Coast (Velasco et al., 2015).

Given the above evidence, each climate index tends to differently impact different oscillation modes of groundwater levels. AMO's significant effect is observed at interdecadal and annual modes while PDO's highest effect is related to decadal and interdecadal ones. The highest influence of ENSO is observed across the decadal and middle-interannual whereas for NAO, the highest coherence patterns are remarked at annual and interdecadal frequency bands. It is likely apparent that the results from each index well correspond to its dominant power spectrums highlighted in Fig. 3. As an example, the middle-interannual and decadal modes are the dominant signals in the local and global CWTs for ENSO (i.e., SOI). Overall, it is found that the decadal and interdecadal signals are the dominant modes in the climate indices, particularly PDO, AMO, and ENSO (Figs. 5 and S3), consistent with the dominant power regions in the CWT for the majority of aquifers (Fig. 3). It is found that PDO (with the mean coherence of 0.51) has the highest influence on groundwater fluctuations over Iran compared to the other three indices of AMO (0.45), ENSO (0.42), and NAO (0.34). This well agrees with those results obtained by Rezaei and Gurdak (2020) for the aquifers in the Lake Urmia watershed.

Despite similarity between the teleconnections observed in the majority of aquifers in this study and those in the surface hydroclimate (precipitation, drought, rivers, etc.) in the literature, it is here observed that ENSO has the lowest effect on the annual oscillation modes in the groundwater

394 levels while most of the previous results found that ENSO is one of the most important indices
395 modulating Iran hydroclimate variability (but not groundwater) (e.g., Alizadeh-Choobari and Najafi,
396 2018; Ahmadi et al., 2019; Alizadeh-Choobari and Adibi, 2019; Rezaei and Gurdak, 2020). We further
397 observed that the groundwater variability, particularly low-frequent one, is more correlated with
398 lower frequent climate circulations such as PDO and AMO, rather than ENSO. This is possibly raised
399 by the unsaturated zone contribution in damping and lagging the climate variability signals. In fact,
400 the higher-frequency signals of ENSO (i.e., SOI) and NAO damp through the unsaturated zone greater
401 than the lower-frequency indices (Bloomfield & Marchant, 2013; Van Loon, 2015; Van Loon et al.,
402 2014; Rust et al., 2018). While this phenomenon doesn't exist in other hydroclimate variables (e.g.,
403 precipitation, temperature, surface soil-moisture, and drought), so that, the aquifer teleconnections
404 may relatively different from those observed in precipitation, drought, and temperature (Velasco et
405 al., 2015). To clarify this issue in our case, Fig. 7 shows the coherence values averaged across the
406 annual, 2-4-, 4-6-, and 8-12-yr frequency bands versus mean water table depth for each aquifer. It is
407 observed that the coherence values are generally smaller in the deeper aquifers (i.e., regression lines
408 have a negative slope), particularly for the annual signals which have a higher frequency (Fig. 7a).
409 Furthermore, the highest coherence patterns between AMO and groundwater levels across 1-yr
410 periodicity have occurred at the shallowest aquifers of 2, 4, 8b, and 5 with water table depths of <10
411 m. On the contrary, the lowest coherence between AMO and annual oscillation modes is observed in
412 aquifers 14, 9a, 10a, and 11 that are located in central Iran and eastern parts of the country with
413 deeper aquifers and drier climates (Fig. S1). In fact, damping and lagging the climate variability
414 signals are higher through the thicker unsaturated (i.e., deeper water table) zones, particularly those
415 of lower hydraulic conductivities (Rust et al., 2018). Likewise, it is found that shallower aquifers
416 receive greater amplitude of NAO signals across Europe (Rust et al., 2018). Furthermore, as the
417 frequency of the signals increases, the slope of the fitted-lines also tends to increase that is the slope
418 of the 1-yr oscillation modes (Fig. 7a) is greater than that of the lower frequency signals of

interannual and decadal modes (Figs. 7b to 7d). We therefore concluded that the higher-frequency signals are damped more than the lower-frequency modes across the Iranian aquifers.

5.2. Multiple interacting controls of climate indices:

Comparing Figs. 4a, 4b, 4c, S3, and S4 indicates that the coupled indices and the groundwater levels have stronger and broader significant coherence patterns for the aquifers compared to each individual index, suggesting that multiple interacting control of indices can better predict the water table behavior across the country. As an example, comparison of the WTCs and MWTCs results respectively from each individual index (Fig. S3) and three-coupled (Fig. S4) indices for each particular aquifer show that coherence patterns in Fig. S4 are largely stronger and broader than those in Fig. S3, where the colors tend to be more in yellow (higher coherence values) in Fig. S4. Figs. 4a, 4b and 4c also reveals that the three-coupled indices, on the whole, have larger mean coherence values than both the two-coupled indices and each individual index for all the aquifers across the country. However, among the two-coupled indices, the PDO+SOI index has the highest effect on groundwater levels at the short-interannual, decadal, and interdecadal oscillation modes while the annual and middle-interannual frequency signals are more modulated by the AMO+PDO index (Fig. 4b). Fig. 4b also shows that the Pacific-based indices (PDO+SOI with mean coherence value of 0.74) have a stronger effect on Iran's aquifers than the Atlantic-based (AMO+NAO with mean coherence value of 0.70), consistent with the findings made from the integrated precipitation and soil-moisture across Iran (Rezaei, 2021). Among the three-coupled ones, except for annual signals in groundwater levels which are correlated with AMO+NAO+PDO, all the other dominant signals from interannual to interdecadal are more correlated to the three-coupled AMO+PDO+SOI index (Fig. 4c). Consequently, the combination of AMO+PDO+SOI presents the best ability to explain the natural groundwater variability in Iran. Wang et al. (2014) also stated that the La Nina coupled with cold PDO have highly affected the severe droughts across the Fertile Crescent owing to anomalous ridging across eastern Europe and northern Asia and subsidence over Fertile Crescent itself.

5.3. Temporal changes in teleconnections:

The WTC results demonstrate that, similar to different frequency bands, the teleconnection patterns for different time periods are different because of temporal differences in both the ocean-atmospheric circulations and in groundwater demand by humans and groundwater-dependent ecosystems (Klove et al., 2014). As a case example, Fig. 5 reveals that the imprint of AMO on groundwater levels of aquifers 1c, 6b, and 8b has substantially increased after 2003. Likewise, Rust et al. (2018) pointed out that the low-frequency signals in the groundwater levels have both spatial and temporal variability. We therefore scrutinize the coherence variations over time by averaging the coherence value across all the frequency bands to obtain the mean coherence value at different times (Fig. 8). In Fig. 8, the mean standard deviation for ENSO, PDO, AMO and NAO are estimated to be 0.09 (0.01-0.15), 0.10 (0.02-0.14), 0.10 (0.01-0.15), and 0.07 (0.03-0.12), respectively. Some important observations that can be made from Fig. 8 are as follows.

First, although the Pacific-basic indices of PDO and ENSO, on the whole, have a higher correlation with Iran's groundwater compared to Atlantic-based indices of AMO and NAO, their teleconnections have significantly weakened after 2000. PDO and ENSO's lowest coherence values are observed from 2003 to 2012, particularly in aquifers 2, 3, 7c, 8a, 8b, 9a, 10b, and 12 as shown in Fig. S3. Likewise, Rajagopalan et al. (1997) pointed out that the influence of ENSO on Middle Eastern precipitation has become remarkably strong during the two last decades of the 20th century, in part due to variations in the frequency and intensity of ENSO occurrences since the mid-1970s. Although the teleconnections tend to gradually strengthen after 2010 again, it is still weaker than that observed before 2000 for PDO and ENSO indices. Notably, during 1976-1980, a relative decrease in coherence between indices and water table in Iran is also observable in both Fig. 9 and S3 (especially, in the interannual and decadal oscillation signals at the WTCs for aquifers 1a and 7b). A weakness in coherence observed over 2003-2012 may result from either the natural fluctuations or thickening the unsaturated zone during the two last recent decades resulting from over-extraction from

aquifers, severe water table dropping, and more frequent occurrences of severe drought events across Iran (Rezaei and Mohammadi, 2017; Ahmadi et al., 2018). However, this issue still needs more investigation that is out of the scope of this paper.

Second, unlike the Pacific-based indices, relative effects of the Atlantic-based ones (AMO and, to lesser magnitude, NAO) on Iran's groundwater tend to strengthen after 2000. The AMO's influence has reached its maximum at a period from 2010 to 2019 (Fig. 9). Fig. S3 clearly show that this strengthen in AMO's coherence with water levels are more apparent in the annual frequency bands at the WTCs of the majority of aquifers such as 1a, 1b, 1c, 2, 3, 4, 5, 6b, and 6c. Fig. S2 demonstrates that unlike the latest 30-year of the 19th century, AMO turned to its positive (warm) phase after 2000 and remains near the constant value on average, signifying that the positive AMO has possibly stronger effects on Iranian aquifers. Ahmadi et al. (2018) pointed out that both the frequency of droughts and the temperature over Iran increased since 2000 coincided with the start of the warm (positive) phase of AMO.

Third, it seems that the Iranian aquifers respond to droughts periods sooner than the wet periods. Rezaei (2021) determined that 1998-2000, 2007-2009, and 2011-2012 (yellow boxes in Fig. 8) are the most severe droughts across the country since 1979 that largely coincided with the strong La Nino phases. Interestingly, the SOI (i.e., ENSO) curve in Fig. 8 shows relative peaks coincided with these severe drought years, signifying quick aquifers' response to droughts in comparison with the wet periods. As an example, during the severe 1998-2000, 2007-2009, and 2010-11 droughts corresponding to the historical strong La Nina in 2007-08 and 2010-11 (Rezaei, 2021), moderate to strong coherence patterns are observed around the 1-2-yr periods at WTCs between ENSO and water levels for aquifers of 1a, 1c, 3, 4, 5, 6a, 6b, 6c, 7a, 7b, 8b, 9a, 9c, 10a, 11, 13, and 14. There further is a significant power region in the CWTs of ENSO across ~2-yr periods from 2007-2012, confirming the strong coherence patterns in the above aquifers. This relatively quick aquifers response to droughts effect is most probably resulted from the over-excretion from groundwater in the following dry

494 season exacerbating the drought effect. Notably, pumping from groundwater is the primary annual
495 discharge components for Iranian aquifers (Rezaei and Mohammadi, 2017; Mirzaei et al., 2019).
496 Furthermore, unlike the recharge phenomena, the discharge by pumping circumvents the
497 unsaturated zone roles in damping and lagging the discharge signals. The recharge dominantly
498 occurs by natural phenomena through the unsaturated zone while the discharge from Iranian
499 aquifers dominantly is controlled by pumping without significant effect of the unsaturated zone.
500 Notably, detrending the groundwater level series by subtracting a regression-fitted low-order
501 polynomial, explained in the methodology, may not be able to remove the annual anthropogenic
502 signals completely. Otherwise, the recharge shock during the wet years may percolate to water table
503 with longer time delay and more damping compared to the drought periods, particularly in the
504 deeper aquifers with higher potential in signal attenuation (Bloomfield & Marchant, 2013; Van Loon,
505 2015; Van Loon et al., 2014; Rust et al., 2018).

506 **5.4. Data length effect on teleconnections:**

507 The data length can significantly affect the total coherence patterns and, in turn, our
508 understanding of teleconnections since the above evidence reveals that the climate indices
509 teleconnections with groundwater series change over time. This study shows that the data length can
510 significantly affect the results if the time series are not contemporaneous and only one value of
511 coherence/correlation is obtained from a particular series instead of separate computation for
512 different frequency bands and different time spans. As an example, Fig. 9 shows the relationship
513 between the mean total coherence values and data length for the four aquifer groups G1 to G4 (from
514 northwest Iran to southern coasts of the Caspian Sea) and G8 to G11 (from east-center to the
515 northern coasts of the Persian Gulf). Here, those adjacent aquifers are used for plotting the data
516 length-coherence curves as it is anticipated that adjacent aquifers show similar teleconnections. The
517 regression fitted lines with R^2=0.95 for G1 to G4 and R^2=0.80 for G8 to G11 (Fig. 9) demonstrate that
518 the mean coherence is substantially affected by data length: the larger values obtained from longer

519 data lengths. Consequently, those teleconnections that are only assessed by the results from either
520 mean coherence or correlation values ignoring the time specific may not be reasonable except for the
521 contemporaneous time series. Therefore, wavelet analyses used in this study are reasonable since
522 different coherence values are computed across the different frequency and time bands for each
523 water level series. Finally, this work suggests that the wavelet analysis can better than the simple
524 correlation analysis assess the teleconnections, particularly when the data lengths from different
525 locations/stations are not contemporaneous. The correlations computed over the whole time span
526 would not provide effective information (Yuan et al., 2016).

527 **6. Conclusions:**

528 The main findings made in this study are as follows:

529 - The significant coherence patterns between the climate indices and groundwater levels, on the
530 whole, occurred at five frequency bounds of the annual (~1-yr), short-interannual (2-4-yr), middle-
531 interannual (4-6-yr), decadal (8-12-yr), and interdecadal (14-18-yr), consistent with the dominant
532 modes obtained from the CWT analyses.

533 - The annual variability largely correlates to AMO (mean coherence value of 0.58) and, to lesser
534 magnitude, PDO (0.47) and NAO (0.45). Both the interannual and decadal oscillation signals in the
535 groundwater levels are more correlated with the Pacific-based indices of PDO and ENSO rather than
536 the Atlantic-based indices of AMO and NAO. The interdecadal modes are more affected by the lower-
537 frequency indices of AMO (0.71) and PDO (0.62) rather than the higher-frequency indices of ENSO
538 (0.29.) and NAO (0.29).

539 - The ocean-atmospheric circulations have the highest footprints on the Zagros and upper latitude
540 regions of the country characterized by the shallowest water table, highest precipitation, and lowest
541 temperature. The lowest teleconnections are rather observed in the aquifers of the southeastern,
542 central, and eastern parts with thicker unsaturated zones and drier conditions.

- The influence of each climate index varies much over different modes of groundwater levels. AMO's significant effect is observed at interdecadal and annual modes while PDO's highest effect is related to decadal and interdecadal. The highest influence of ENSO is observed across the decadal and interannual whereas the NAO's highest coherence patterns are remarked at annual and interdecadal frequency bands.

- Given the larger damping and lagging effect of unsaturated zone on the higher frequency modes, the groundwater variability is more correlated with lower frequent climate circulations such as PDO and AMO, rather than ENSO.

- The Pacific-basic indices of PDO and ENSO generally have a higher correlation with Iranian aquifers compared to Atlantic-based indices of AMO and NAO. Notably, influences of the Pacific-based indices on Iranian aquifers have weakened after 2000 while relative effects of the Atlantic-based ones tend to strengthen after 2000, particularly after 2010.

- It is also observed that the aquifers respond to droughts sooner than the wet periods, most probably resulted from the over-excretion from groundwater that immediately started at the dry season of severe droughts exacerbating the drought's impact and circumventing the damping and lagging effects of the unsaturated zones.

- Multiple interacting effects of AMO+PDO+SOI can better modulate the annual to interdecadal groundwater level variability. This enhanced understanding of the influence of multiple interacting from atmospheric processes observed here would be immensely beneficial for improving the state-of-the-art aquifer behavior prediction.

- Finally, this study shows that the data length can significantly affect the teleconnections results if the time series are not contemporaneous and only one value of coherence/correlation is computed for all the data length instead of separate computations for different frequency bands and different time spans.

Notably the wavelet analysis results would be strengthened with additional years of data by capturing the multidecadal modes, but the overall patterns in the higher frequency bands would likely remain with longer-term signals. However, this study reveals that understanding annual to interdecadal behavior in the natural large-scale climate is a universally valuable factor in the long-term predictability of groundwater storage variations and conducting effective groundwater management strategies.

Conflict of Interest:

The author declare that he has no conflict of interest.

Funding Statement:

This research is financially supported by my own means.

Author's Contribution:

Abolfaz Rezaei conceptualized the work, did the data analysis and methodology, and wrote the paper.

Availability of data and material:

The groundwater data used in this study are available in http://wrs.wrm.ir/amar/login.asp, upon requestion. The monthly time series of the climate indices of AMO, Nao, PDO, and ENSO were downloaded from NOAA, https://www.ncdc.noaa.gov/teleconnections.

Ethics approval:

The author confirms that this article is original research and has not been published or presented previously in any journal or conference in any language (in whole or in part).

Acknowledgements:

We would like to thanks Dr. Arash Nadri from Arizona Department of Water Resources for initial review of the paper. We also thank Iran Water Resources Management Company (IWRMC), Tehran, particularly Dr. Rohollah Adinehvand, for providing the representative groundwater levels.

References:

Abbasi, M., Maleki, S.M., 2017. Iranian surface air temperature periodicities and correlations with the North Atlantic and Indian Ocean sea surface temperature variations. Meteorol. Appl. 24 (2), 268–275.

Ahmadi, M., Salimi, S., Hosseini, S.A., Poorantiyosh, H., Bayat, A., 2019. Iran's precipitation analysis using synoptic modeling of major teleconnection forces (MTF). Dynam. Atmos. Ocean 85, 41–56.

Alijani, B., 2000. Iran Climatology. Payam Nour Publication, Tehran, Iran. ISBN 978-964-455-621-0.

Alizadeh-Choobari, O., Adibi, P., 2019. Impacts of large-scale teleconnections on climate variability over Southwest Asia. Dynam. Atmos. Ocean 86, 41–51.

Alizadeh-Choobari, O., Najafi, M.S., 2018. Climate variability in Iran in response to the diversity of the El Niño-Southern Oscillation. Int. J. Climatol. 38(11), 4239-4250.

Bloomfield, J.P. & Marchant, B.P., 2013. Analysis of groundwater drought building on the standardised precipitation index approach. Hydrol. Earth Syst. Sci. 17(12), 4769–4787.

Cayan, D.R., Webb, R.H., 1992. El Niño Southern Oscillation and streamflow in the western United States. In: Diaz, H.F., Markgraf, V. (Eds.), El Niño: Historical and Paleoclimatic Aspects of the Southern Oscillation. Cambridge University Press, New York, N.Y, pp. 29–68.

610 Dickinson, J.E., Hanson, R.T., Predmore, S.K., 2014. HydroClimATe—Hydrologic and Climatic Analysis
611 Toolkit: U.S. Geological Survey Techniques and Methods 4–A9, 49 p,
612 <http://dx.doi.org/10.3133/tm4a9>.

613 Green, T., Taniguchi, M., Kooi, H., Gurdak, J.J., Hiscock, K., Allen, D., Treidel, H., Aurelia, A., 2011.
614 Beneath the surface of global change: impacts of climate change on groundwater. J. Hydrol.
615 405, 532–560.

616 Grinsted, A., Moore, J.C., Jevrejeva, S., 2004. Application of the cross wavelet transform and wavelet
617 coherence to geophysical time series. Nonlinear Process. Geophys. 11 (5), 561–566.

618 Juanxiong, H., Zhihao, Y., & Xiuqun, Y., (2004). Temporal characteristics of Pacific Decadal Oscillation
619 (PDO) and ENSO and their relationship analyzed with method of Empirical Mode
620 Decomposition (EMD). J. Meteorol. Res. 19, 83-92.

621 Hadi Pour, S., Abd Wahab, A. K., Shahid, S., & Wang, X., 2019. Spatial pattern of the unidirectional
622 trends in thermal bioclimatic indicators in Iran. Sustainability 11(8), 2287.

623 Hanson, R.T., Dettinger, M.D., Newhouse, M.W., 2006. Relations between climatic variability and
624 hydrologic time series from four alluvial basins across the southwestern United States.
625 Hydrogeol. J. 14, 1122–1146.

626 Hanson, R.T., Newhouse, M.W., Dettinger, M.D., 2004. A methodology to assess relations between
627 climatic variability and variations in hydrologic time series in the southwestern United States.
628 J. Hydrol. 287 (1–4), 252–269.

629 Holman, I.P., Rivas-Casado, M., Bloomfield, J.P. & Gurdak, J.J., 2011. Identifying nonstationary
630 groundwater level response to North Atlantic ocean-atmosphere teleconnection patterns
631 using wavelet coherence. Hydrogeol. J. 19(6), 724 pp.1269–1278.

Hu, W., Si, B.C., 2016. Multiple wavelet coherence for untangling scale-specific and localized multivariate relationships in geosciences. Hydrol. Earth Syst. Sci. 20(8), 3183.

Hurkmans, R., Troch, P.A., Uijlenhoet, R., Torfs, P., Durcik, M., 2009. Effects of climate variability on water storage in the Colorado River basin. J. Hydrometeorol. 10(5), 1257–1270.

Klove, B., Ala-Aho, P., Bertrand, G., Gurdak, J.J., Kupfersberger, H., Kvaerner, J., Muotka, T., Mykra, H., Preda, E., Rossi, P., Uvo, C.B., Velasco, E., Wachniew, P., Velazquez, M.P., 2014. Climate change impacts on groundwater and dependent ecosystems. J. Hydrol. 518, 250-266.

Kuss, A.J.M., Gurdak, J.J., 2014. Groundwater level response in US principal aquifers to ENSO, NAO, PDO, and AMO. J. Hydrol. 519, 1939–1952.

McMahon, P.B., Dennehy, K.F., Bruce, B.W., Böhlke, J.K., Michel, R.L., Gurdak, J.J., Hurlbut, D.B., 2006. Storage and transit time of chemicals in thick unsaturated zones under rangeland and irrigated cropland, High Plains, United States. Water Resour. Res. 42.

Mohammadrezaei, M., Soltani, S., Modarres, R., 2020. Evaluating the effect of ocean-atmospheric indices on drought in Iran. Theor. Appl. Climatol., 1-12.

Mirzaei, A., Saghafian, B., Mirchi, A., Madani, K., 2019. The groundwater–energy–food nexus in Iran's agricultural sector: implications for water security. Water 11(9), 1835.

Newman, M., Compo, G.P., Alexander, M.A., 2003. ENSO-forced variability of the Pacific Decadal Oscillation, J. Clim. 16, 3853–3857.

Notaro, M., Yu, Y., Kalashnikova, O.V., 2015. Regime shift in Arabian dust activity, triggered by persistent Fertile Crescent drought. J. Geophys. Res. Atmos. 120 (19).

Perez-Valdivia, C., Sauchyn, D., Vanstone, J., 2012. Groundwater levels and teleconnection patterns in the Canadian Prairies. Water Resour. Res. 48(7).

654 Rajagopalan, B., Lall, U., Cane, M.A., 1997. Anomalous ENSO occurrences: An alternative view. J. Clim.
655 10, 2351–2357.

656 Rezaei, A. 2020. Chemistry of the karst Sarabkalan Spring, Iran, and controls of PDO and ENSO climate
657 indices on it. Groundwater. https://doi.org/10.1111/gwat.13034.

658 Rezaei, A., 2021. Ocean-atmosphere circulation controls on integrated meteorological and
659 agricultural drought over Iran. Resubmitted to J. Hydrol.

660 Rezaei, A., Gurdak, J.J., 2020. Large-scale climate variability controls on climate, vegetation coverage,
661 lake and groundwater storage in the Lake Urmia watershed using SSA and wavelet analysis.
662 Sci. Total Environ., 138273.

663 Rezaei, A., Mohammadi, Z., 2017. Annual safe groundwater yield in a semiarid basin using
664 combination of water balance equation and water table fluctuation. J. Afr. Earth Sci. 134, 241-
665 248.

666 Ropelewski, C.F., Halpert, M.S., 1986. North American precipitation and temperature patterns
667 associated with the El Niño/Southern Oscillation (ENSO). Mon. Weather Rev. 114 (12), 2352–
668 2362.

669 Rust, W., Holman, I., Bloomfield, J., Cuthbert, M., Corstanje, R., 2019. Understanding the potential of
670 climate teleconnections to project future groundwater drought. Hydrol. Earth Syst. Sci. 23,
671 3233–3245.

672 Rust, W., Holman, I., Corstanje, R., Bloomfield, J., Cuthbert, M., 2018. A conceptual model for climatic
673 teleconnection signal control on groundwater variability in Europe. Earth-Sci. Rev. 177, 164-
674 174.

675 Rust, W., Corstanje, R., Holman, I.P. & Milne, A.E., 2014. Detecting land use and land management
676 influences on catchment hydrology by modelling and wavelets. J. Hydrol. 517, 378–389.

677 Sadoff, C., Muller, M., 2009. Water Management, Water Security and Climate Change Adaptation: Early
678 Impacts and Essential Responses. Global Water Partnership, Stockholm.

679 Schulte, J.A., 2019. Statistical hypothesis testing in wavelet analysis: theoretical developments and
680 applications to Indian rainfall.

681 Torrence, C., Compo, G.P., 1998. A practical guide to wavelet analysis. Bull Am. Meteorol. Soc. 79, 61–
682 78.

683 Torrence, C., Webster, P.J., 1999. Interdecadal changes in the ENSOmonsoon system. J. Clim. 12, 2679–
684 2690.

685 Treidel, H., Martin-Bordes, J.L., Gurdak, J.J. (Eds.), 2012. Climate Change Effects on Groundwater
686 Resources: A Global Synthesis of Findings and Recommendations. CRC Press, Taylor & Francis
687 Group, London, UK.

688 Walvoord, M.A., Phillips, F.M., Stonestrom, D.A., Evans, R.D., Hartsough, P.C., Newman, B.D., Striegl,
689 R.G., 2003. A reservoir of nitrate beneath desert soils. Science 302, 1021–1024

690 Van Loon, A.F., 2015. Hydrological drought explained. Wiley Interdisciplinary Reviews: Water 2(4),
691 359–392.

692 Van Loon, A.F., Tijdeman, E., Wanders, N., Van Lanen, H.A.J., Teuling, A.J. & Uijlenhoet, R., 2014. How
693 climate seasonality modifies drought duration and deficit. J. Geophys. Res. Atmos.
694 119(8),4640–4656.

695 Velasco, E. M., Gurdak, J. J., Dickinson, J. E., Ferré, T. P. A., Corona, C.R., 2015. Interannual to
696 multidecadal climate forcings on groundwater resources of the US West Coast. J. Hydrol. Reg.
697 Stud. 11, 250-265.

698 Vicente-Serrano, S.M., López-Moreno, J.I., Gimeno, L., Nieto, R., Morán-Tejeda, E., LorenzoLacruz, J.,
699 Azorin-Molina, C., 2011. A multiscalar global evaluation of the impact of ENSO on droughts. J.
700 Geophys. Res. Atmos. 116 (D20).

701 Wang, S., Huang, J., He, Y., Guan, Y., 2014. Combined effects of the Pacific Decadal Oscillation and El
702 Niño-Southern Oscillation on global land dry-wet changes. Sci. Rep. 4, 6651.

703 Wyatt, M.G., Kravtsov, S., Tsonis, A.A., 2012. Atlantic Multidecadal Oscillation and
704 Northern Hemisphere's climate variability. Clim. Dyn. 38(5–6), 929–949.

705 Yuan, N., Xoplaki, E., Zhu, C., Luterbacher, J., 2016. A novel way to detect correlations on multi-time
706 scales, with temporal evolution and for multi-variables. Sci. Rep. 6, 27707.

707 **Figure captions:**

708 **Fig. 1.** The selected aquifers mapped on the 14 climate zones of Iran presented by Alizadeh-Choobari
709 and Najafi (2018). The black labels refer to climate zones while the blue ones to aquifers.

710 **Fig. 2.** Simple workflow for this study.

711 **Fig. 3.** The local continuous wavelet transform (Local CWT) and its corresponding global power
712 spectrum (GPS) for both the climate indices (AMO, PDO, NAO, and SOI (i.e., ENSO)) and the
713 aquifers' water levels. The thick-black and dotted lines on the local CWT and GPS is the 95%
714 confidence level. For brevity, we only show one aquifer from each aquifer group.

715 **Fig. 4.** The boxplot for the coherence values between groundwater levels and (a) single indices of
716 AMO, PDO, NAO, and ENSO (i.e., SOI), (b) two-coupled indices, and (b) three-coupled indices
717 at significant frequency bands of annual (~1-yr), interannual (2-4- and 4-6-yr), decadal (8-
718 12-yr), and interdecadal (14-18-yr).

719 **Fig. 5.** The wavelet coherence (WTC) between climate indices of AMO, PDO, NAO, and SOI and the
720 representative groundwater levels from the aquifers 1, 6, and 8. The thick black curve is the 5%
721 significance level, and the less intense colors reveal the cone of influence. Black arrows are the

722 phase angle, identifying the phase relation between two series for which right- and left-directed
723 arrows representing in-phase and anti-phase relations, respectively (Grinsted et al., 2004).
724 **Fig. 6.** The climate indices' coherence values averaged over the five dominant frequency bounds from
725 annual to interdecadal across all the country.
726 **Fig. 7.** The mean coherence values versus mean water table depth across different frequency bands
727 of (a) annual 1-yr, (b) short-interannual 2-4-yr, (c) middle-interannual 4-6-yr, and (d)
728 decadal 8-12-yr for each aquifer. Given the limit number of aquifers with long enough times
729 series, the curve for the interdecadal 14-18-yr oscillation mode is not shown.
730 **Fig. 8.** The mean coherence values between the indices and aquifers' water level series in the
731 different time bands across the country. the mean standard deviation for SOI, PDO, AMO and
732 NAO are estimated to be 0.09 (0.01-0.15), 0.10 (0.02-0.14), 0.10 (0.01-0.15), and 0.07 (0.03-
733 0.12), respectively. The orange boxes highlighted the severe historical 1998-2000, 2007-
734 2009, and 2010-2011 droughts across Iran.
735 **Fig. 9.** The mean total coherence value versus the mean data length for aquifer groups (a) G1 to G4
736 and (b) G8 to G9.
737
738
739
740
741
742
743
744
745
746

Fig. 1.

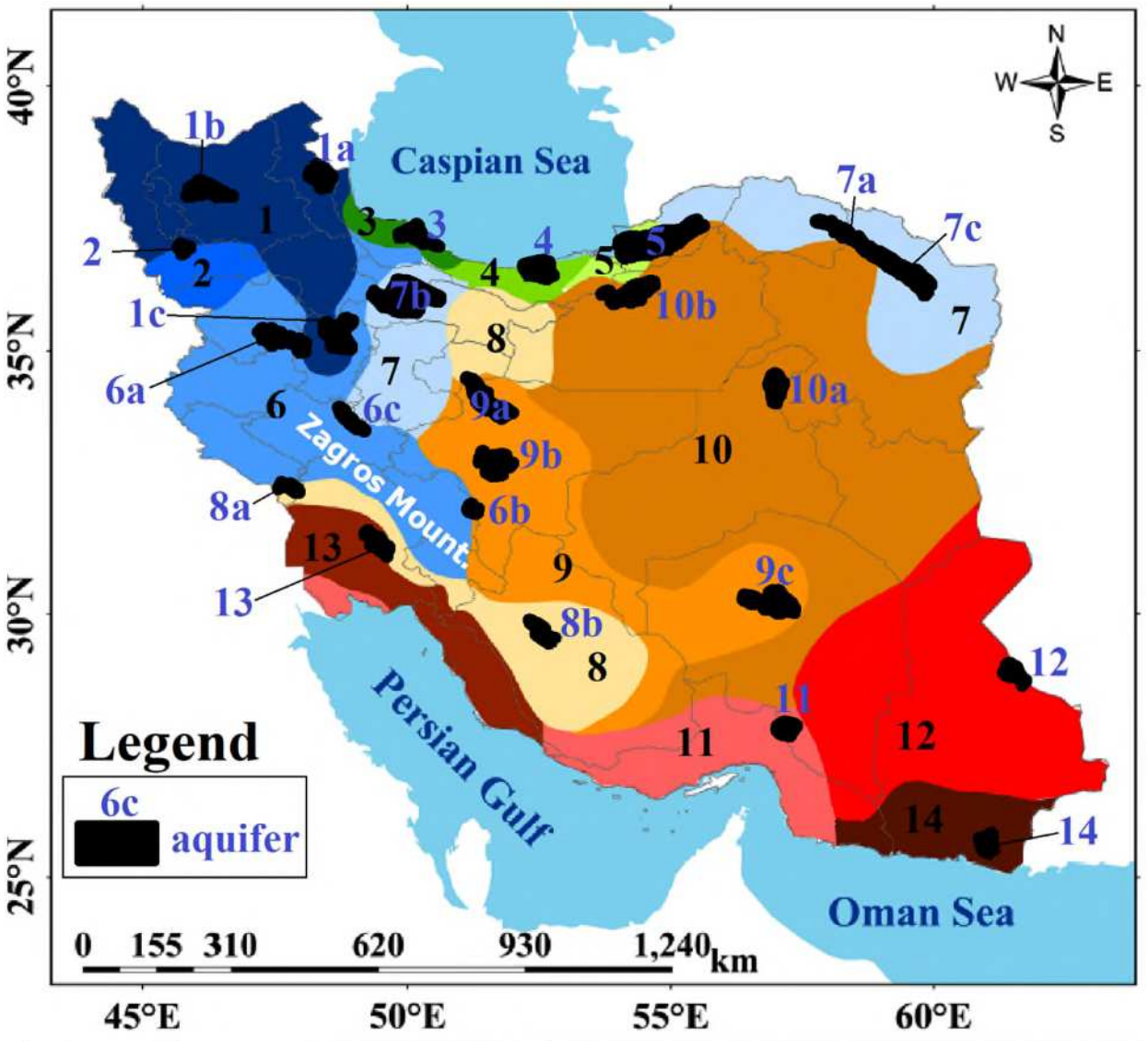

1	Cold and semi-arid	8	Semi-warm and semi-arid
2	Cold and sub-humid	9	Semi-warm and arid
3	Mild and very humid	10	Warm and arid
4	Mild and humid	11	Marine hot and arid
5	Mild and sub-humid	12	Warm and hyper-arid
6	Cool and sub-humid	13	Marine hot and semi-arid
7	Cool and semi-arid	14	Marine warm and arid

761

762

763

764

765

766

767 **Fig. 2.**

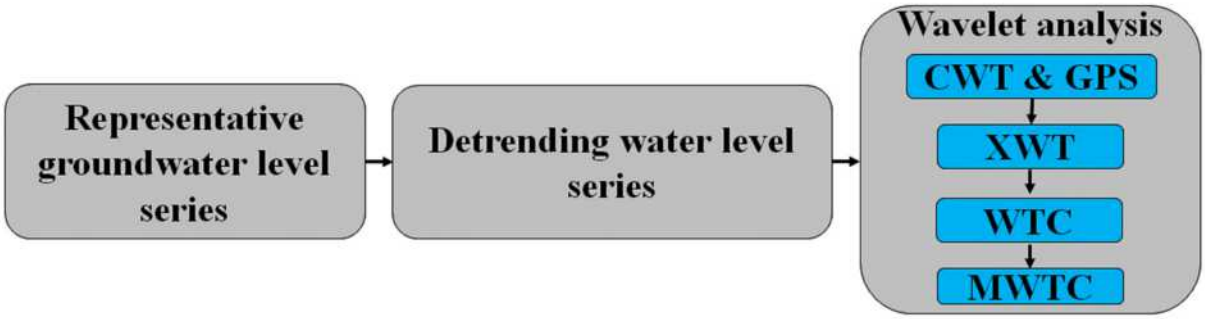

768

769

770

771

772

773

774

775

776

777

778

779

780

781

782

783

784 **Fig. 3.**

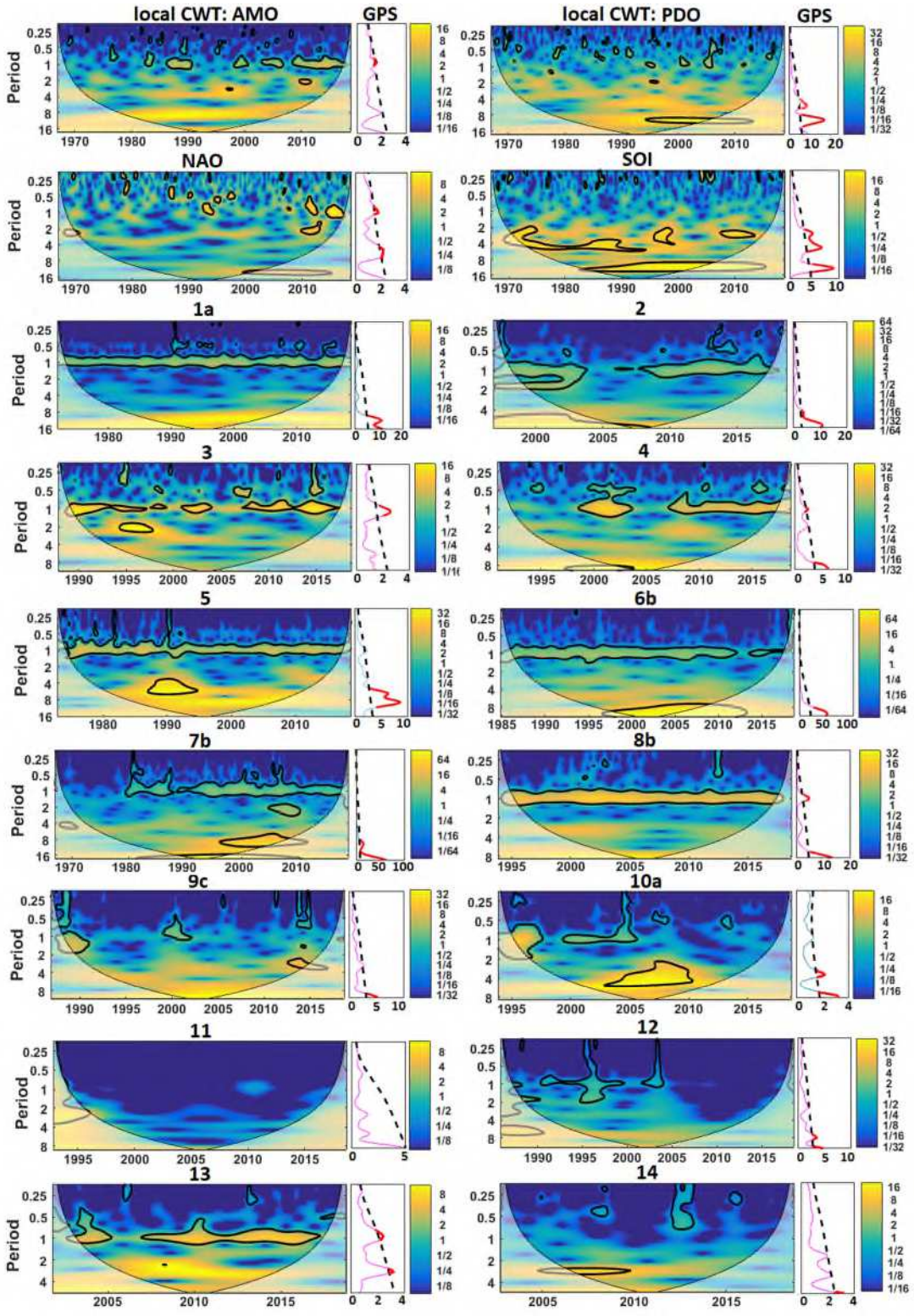

785

786

787 **Fig. 4.**

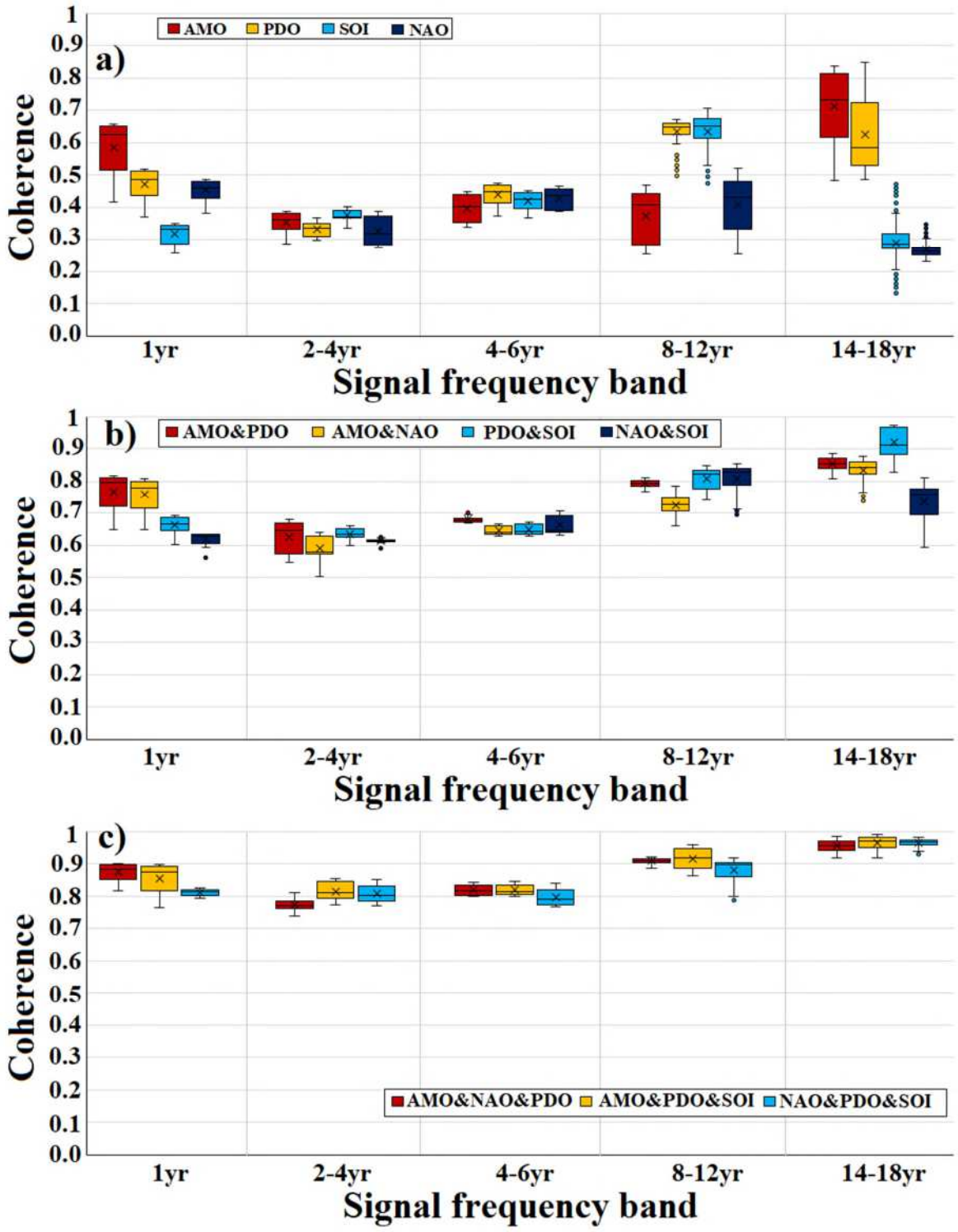

788

789

790

791 **Fig. 5.**

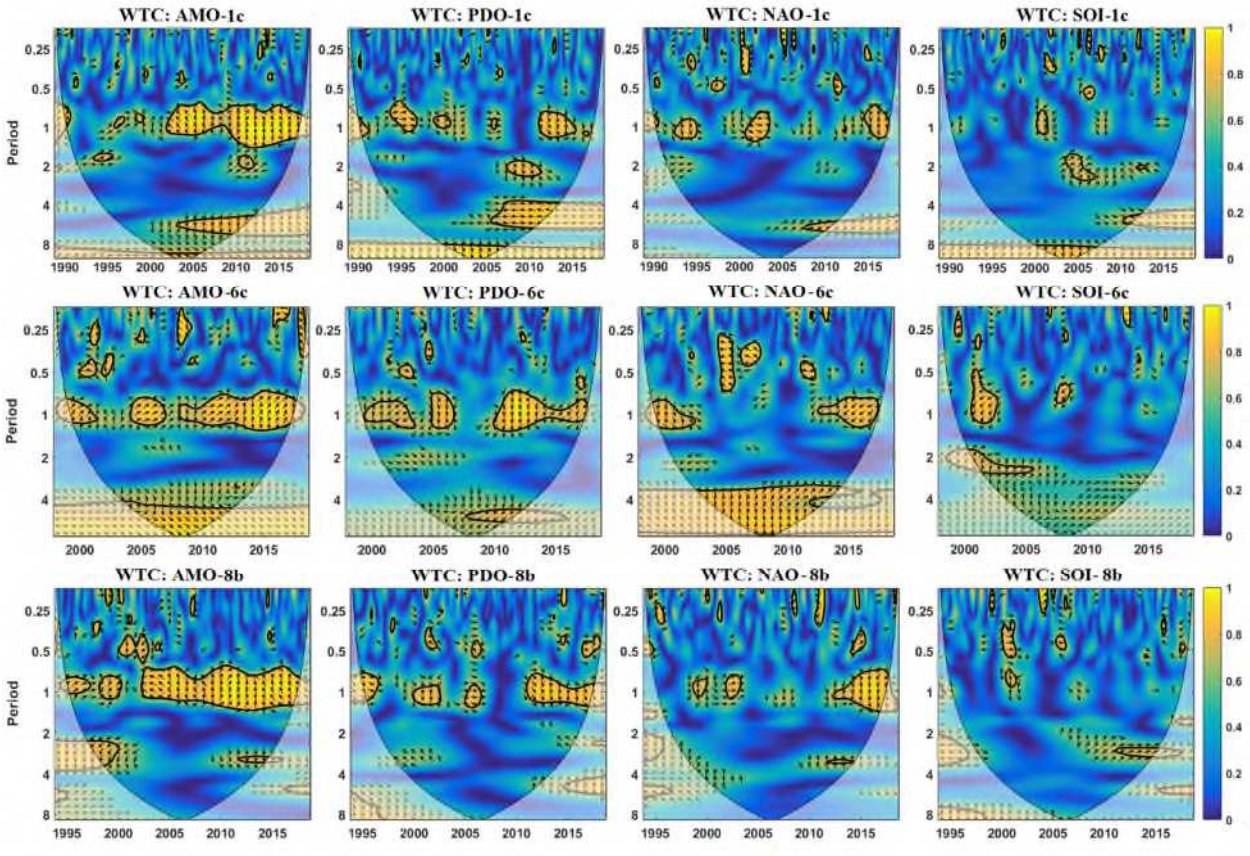
WTC: AMO-1c
WTC: PDO-1c
WTC: NAO-1c
WTC: SOI-1c
WTC: AMO-6c
WTC: PDO-6c
WTC: NAO-6c
WTC: SOI-6c
WTC: AMO-8b
WTC: PDO-8b
WTC: NAO-8b
WTC: SOI- 8b
Period

Fig. 6.

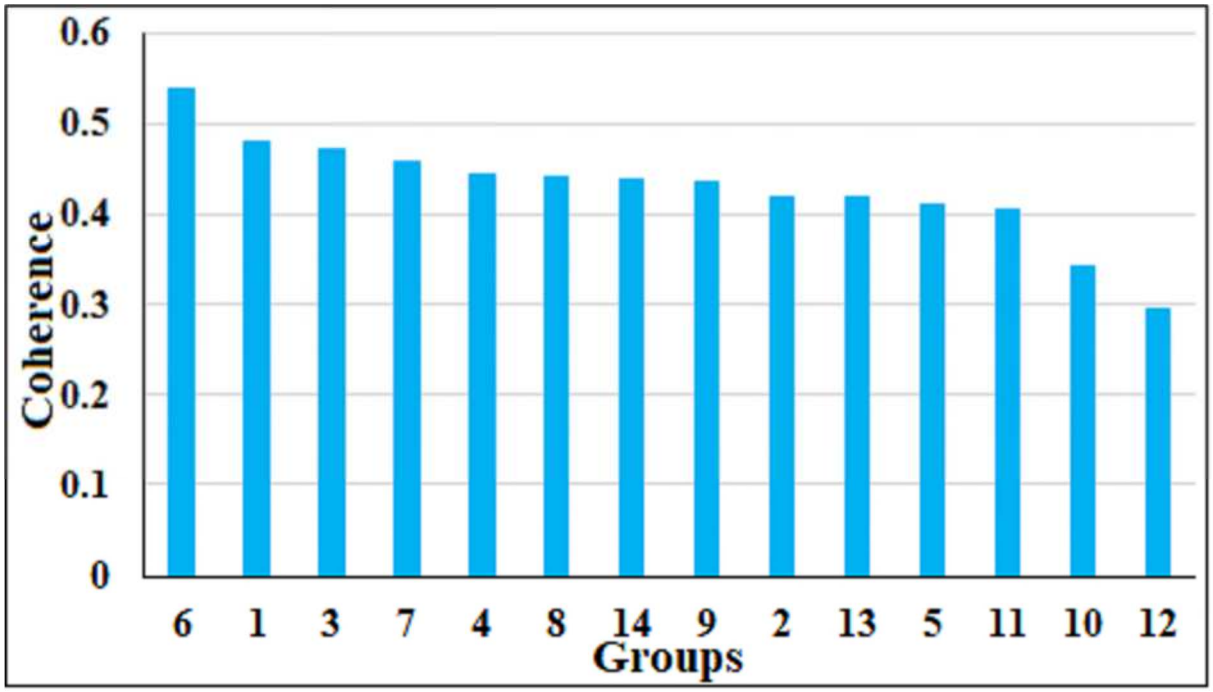

805

806

807 **Fig. 7.**

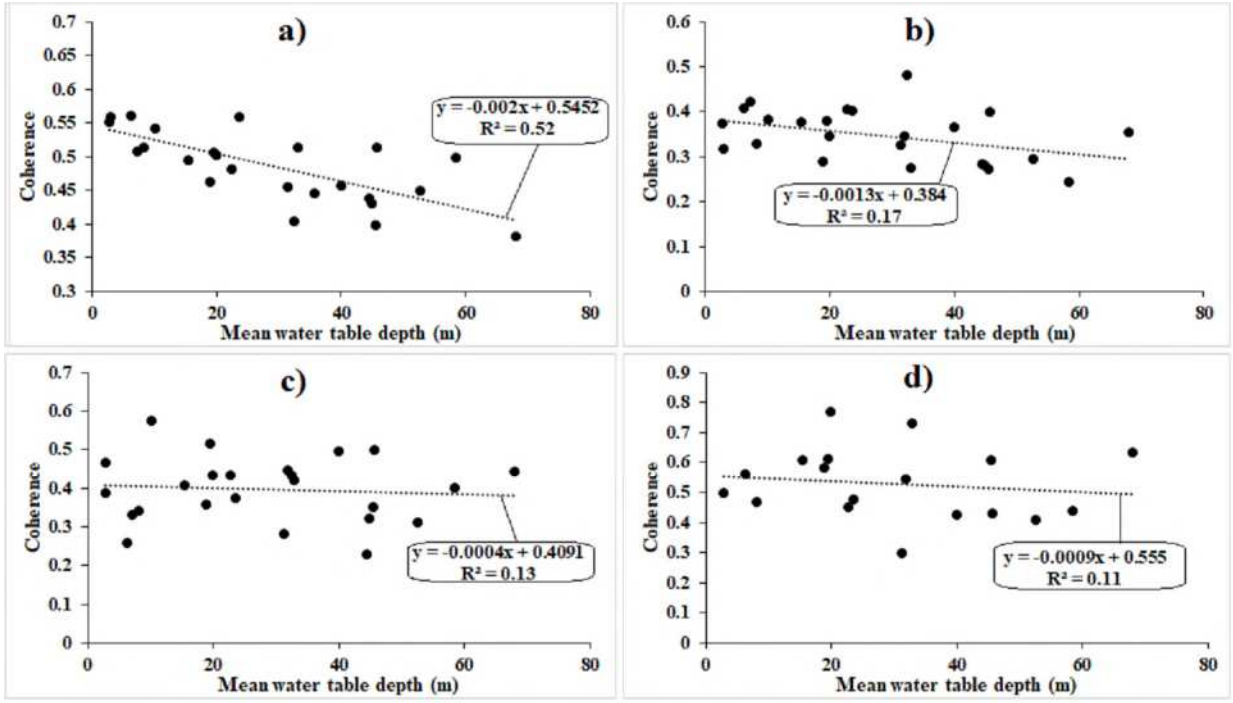

808

809

Fig. 8.

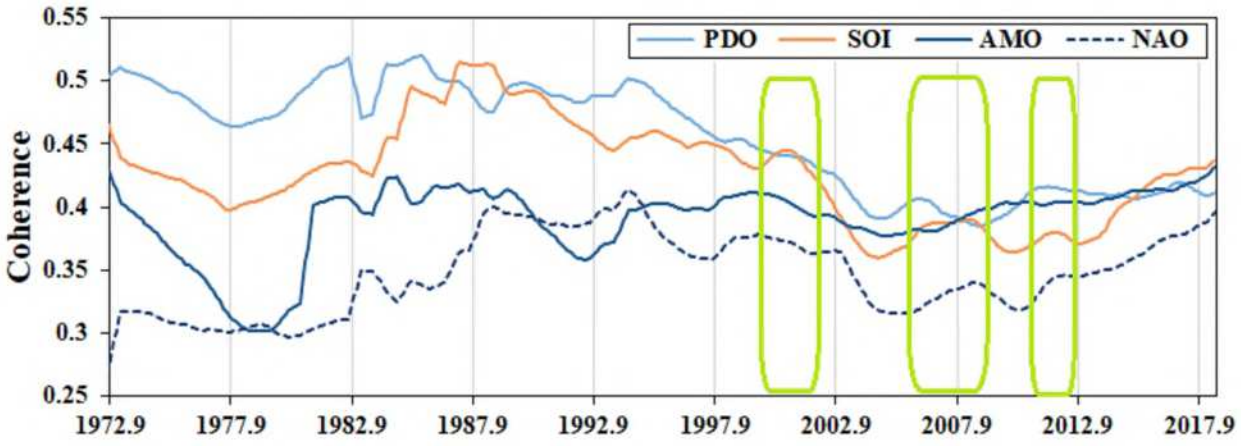
PDO
SOI
AMO
NAO
Coherence
0.55
0.5
0.45
0.4
0.35
0.3
0.25
1972.9
1977.9
1982.9
1987.9
1992.9
1997.9
2002.9
2007.9
2012.9
2017.9

829 **Fig. 9.**

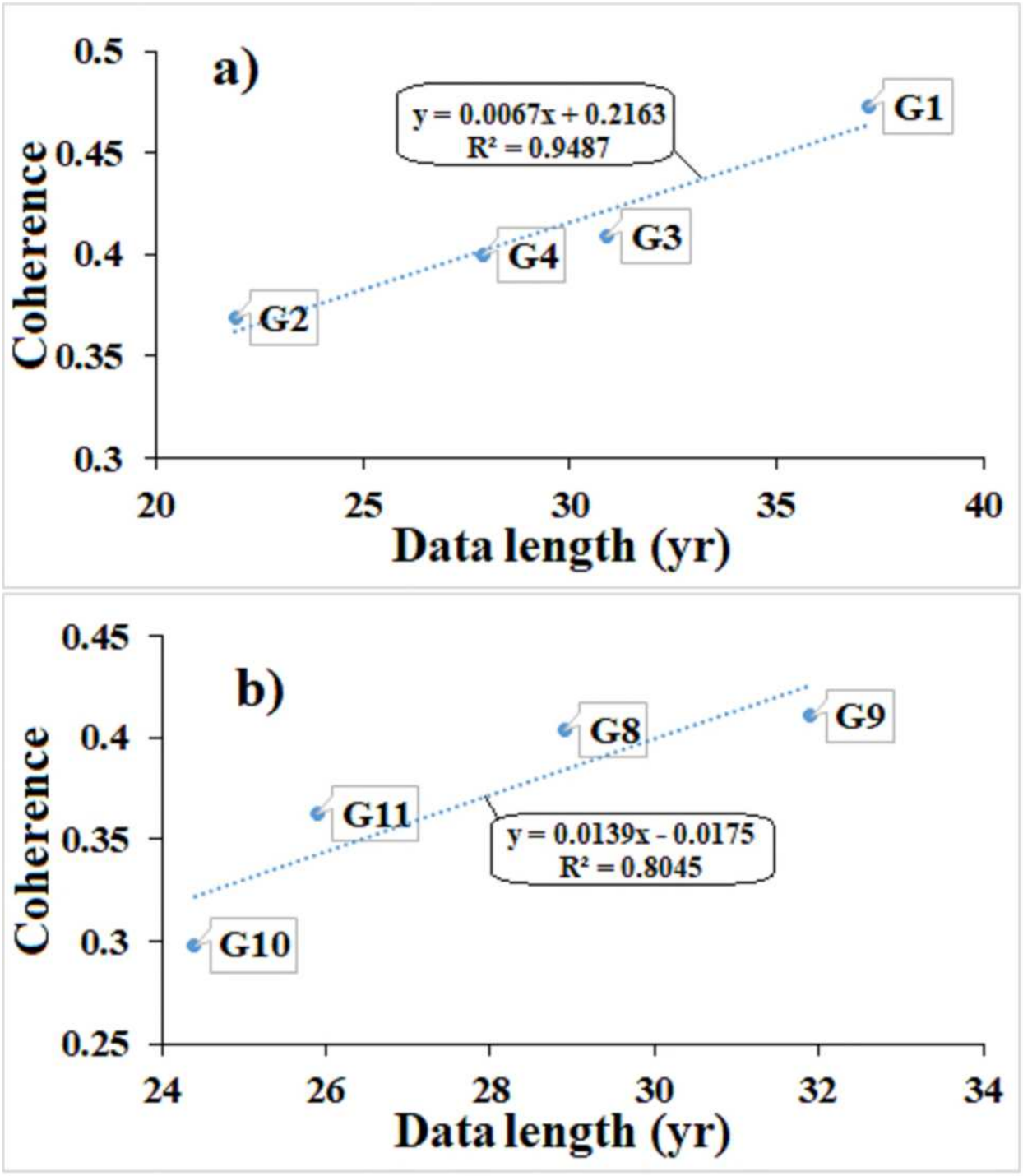
a)
y = 0.0067x + 0.2163
R² = 0.9487
G1
G2
G3
G4
Coherence
Data length (yr)
0.5
0.45
0.4
0.35
0.3
20
25
30
35
40
b)
y = 0.0139x - 0.0175
R² = 0.8045
G8
G9
G11
G10
Coherence
Data length (yr)
0.45
0.4
0.35
0.3
0.25
24
26
28
30
32
34

830

Supplementary Files

This is a list of supplementary files associated with this preprint. Click to download.

- SupportingInfromation.pdf